POLITECNICO DI TORINO
Repository ISTITUZIONALE

Additive manufacturing of PHBH and PBAT biopolymers via fused filament fabrication: a comparison between thermal and thermo-mechanical properties

Original
Additive manufacturing of PHBH and PBAT biopolymers via fused filament fabrication: a comparison between thermal and thermo-mechanical properties / Colucci, G., Fontana, L., Coser, M., Pegoretti, A., Messori, M.. - In: ADVANCES IN MANUFACTURING. - ISSN 2095-3127. - (2026). [10.1007/s40436-026-00622-y]

Availability:
This version is available at: 11583/3016015 since: 2026-09-28T11:39:11Z

Publisher:
Springer Nature

Published
DOI:10.1007/s40436-026-00622-y

Terms of use:

This article is made available under terms and conditions as specified in the corresponding bibliographic description in the repository

Publisher copyright

(Article begins on next page)

26 November 2026

Adv. Manuf.
https://doi.org/10.1007/s40436-026-00622-y

Additive manufacturing of PHBH and PBAT biopolymers via fused filament fabrication: a comparison between thermal and thermo-mechanical properties

Giovanna Colucci[1,2] · Luca Fontana[1] · Mirko Coser[2,3] · Alessandro Pegoretti[2,3] · Massimo Messori[1,2]

Received: 17 October 2025 / Revised: 17 December 2025 / Accepted: 13 July 2026
© The Author(s) 2026

Abstract This study aims to investigate the thermal and thermo-mechanical properties of poly(3-hydroxybutyrate-co-3-hydroxyhexanoate) (PHBH) and poly (butylene adipate-co-terephthalate) (PBAT) as sustainable alternatives for fused filament fabrication (FFF). Starting from commercial pellets, both biopolymers were processed into filaments using an extruder carefully controlling thermal parameters to ensure dimensional consistency. Filaments of PHBH and PBAT were subsequently used to produce several parts by using FFF. Thermal characterization was performed by thermogravimetric analysis (TGA) and differential scanning calorimetry (DSC) measurements to investigate the thermal behaviour of the two biopolymers, while their thermo-mechanical properties were assessed through dynamo-mechanical analysis (DMA) and tensile testing evaluating storage modulus, loss factor, elastic modulus, ultimate tensile strength, and elongation at break. The results evidenced that PHBH's thermal stability slightly decreased progressively from pellet to filament extrusion up to the realization of printed components via FFF, with an important reduction of the degree of crystallinity. PHBH retains high stiffness and strength but remains brittle, limiting its use to applications where rigid components are required. On the contrary, PBAT maintains high thermal stability and thermal transitions quite similar during the whole processing with minor mechanical properties, which makes it useful for applications requiring high flexibility.

Keywords Additive manufacturing (AM) · Fused filament fabrication (FFF) · Biopolymers · Poly(3-hydroxybutyrate-co-3-hydroxyhexanoate) (PHBH) · Poly (butylene adipate-co-terephthalate) (PBAT)

1 Introduction

Additive manufacturing (AM) is a family of manufacturing technologies that enable the creation of 3D components layer-by-layer [1–5]. AM has been utilized across several application fields, such as aerospace [6–8], automotive [6–8] or biomedical [7–9] owing to its capacity to minimize material waste and provide exceptional design versatility [10–13]. Fused filament fabrication (FFF) is one of the most used AM technologies among those available for polymer processing [14], also known as fused deposition modelling (FDM). FFF involves the extrusion of a thermoplastic filament via a heated nozzle, which deposits the polymeric material layer-by-layer to build the final part according to a selected CAD model [15]. The main polymeric materials used for this technology are acrylonitrile-butadiene-styrene (ABS) [16, 17], poly (lactic) acid (PLA) [18], polyamides (PA) [19], thermoplastic polyurethane (TPU) [20], poly (ethylene terephthalate glycol-modified) (PETG) [21]. Among these, PLA is the only one which is biodegradable and derived from renewable resources, aspects that together with its ease of printing make it most favoured for AM [22, 23].

Recent years have witnessed an increasing interest in the development of biopolymers which reduce carbon dioxide emissions and waste amount since they are biodegradable

✉ Giovanna Colucci
giovanna.colucci@polito.it

[1] Dipartimento di Scienza Applicata e Tecnologia (DISAT), Politecnico di Torino, Corso Duca degli Abruzzi 24, 10129 Turin, Italy

[2] National Interuniversity Consortium of Materials Science and Technology (INSTM), Via G. Giusti 9, 50121 Florence, Italy

[3] Department of Industrial Engineering, University of Trento, Via Sommarive 9, 38123 Trento, Italy

Published online: 26 September 2026

and/or biobased [24]. They find applications in biomedical fields, such as tissue engineering and drug delivery systems [25]; they are also widely adopted in food packaging and cosmetics, where biopolymer properties are tailored according to the final applications [26]. In this scenario, merging the use of biopolymers with AM technologies, such as FFF, allows to process environmentally friendly materials with an advanced manufacturing process which is cost and time effective [27].

Poly (3-hydroxybutyrate-co-3-hydroxyhexanoate) (PHBH) is a biopolymer which combines good thermo-mechanical properties with biodegradability, making it suitable for many applications, like tissue engineering and packaging [28]. It is a member of the polyhydroxyalkanoates (PHAs) family, which includes thermoplastic biopolymers synthesized by carbon-rich microorganisms in nutrient-deficient environments [29, 30]. This polymer shows thermoplastic properties and may be processed via standard polymer processing methods, such as cast extrusion and injection moulding [31]. PHBH is recognized for its promising mechanical properties and thermal stability relative to other PHAs, rendering it a suitable choice for AM applications [32]. For example, Kovalcik et al. [33] investigated the possibility to use PHBH for producing scaffolds via FFF, showing good mechanical and viscoelastic properties. PHBH is often used in combination or filled with other materials to improve its final properties. For example, Giubilini et al. [34] successfully produced scaffolds via FFF using PHBH as starting material exploring the possibility of combining it with functionalized cellulose nanocrystals (CNCs) for improving its final mechanical properties.

Valentini et al. [35] investigated mechanical, thermal, and rheological properties of PHBH with fibrillated nanocellulose. Moreover, Ivorra-Martinez et al. [36] studied the possibility of combining PHBH with nanohydroxyapatite (nHA) for scaffold production with FFF system, showing how nHA content can influence the final mechanical properties. In contrast to PHBH, which is entirely bio-based, poly (butylene adipate-co-terephthalate) (PBAT), instead, is a biodegradable fossil-based polymer characterized by a good thermal stability and high elasticity [37], and it is found wide applications in packaging and biomedical fields [38]. It remains biodegradable under certain composting settings [39] and it has been usually utilized in the creation of flexible biodegradable films and coatings mainly for agriculture [40]. It has good potential for sustainable manufacturing [41] and has been investigated for its potential in AM, specifically for FFF technology, where it is frequently combined with other biopolymers, such as PLA to enhance the mechanical characteristics and printability of the final blend [42]. Zhang et al. [43] investigated the processability via FFF of poly (glycolic acid) (PGA) blended with PBAT obtaining good results in terms of thermal behaviour, thermal stability, and mechanical performance. Mechanical testing clearly indicated that FFF 3D-printed samples of PGA/PBAT exhibited comparable tensile, flexural, and impact properties with injection-moulded samples. Jeffri et al. [44] evaluated the processability of PBAT blended with poly(hydroxybutyrate) (PHB), which was a member of PHA family, and this study revealed how PBAT content improved the mechanical performance and processability of PHB material. Moreover, Ali et al. [45] examined the properties of poly(hydroxy-co-3-butyrate-co-3-valerate) (PHBV) blended with PBAT, processed via FFF, with good results showing how PBAT improved ductility of PHBV. Furthermore, Apicella et al. [46] studied the processability of PLA/PBAT/PHBV ternary blend demonstrating how PLA/PBAT blend proportion could influence the processability of PHBV. In the present work, a comparison between PHBH and PBAT thermal and thermo-mechanical properties was studied in detail for a possible use as starting polymeric materials for FFF as AM technology. Starting from raw material pellets, they were first processed into filaments for FFF 3D printing. Because the quality of the filament directly influences the final polymer printability, the dimensional properties of the prepared bio-based filaments were evaluated by measuring filament diameters. Then, the filaments were used to manufacture several test specimens and more complex parts, using FFF as 3D printing technology.

PBAT and PHBH have been individually investigated in several studies related to 3D printing and FFF applications. Our intention was not to overlook this existing body of literature, but rather to underline the lack of a direct comparative study addressing filament production, printability, thermal behaviour, and thermo-mechanical properties within a single experimental framework. The present paper reports a detailed comparison of these two biopolymers processed via FFF, starting from filaments production up to printed specimens manufacturing. Investigating this aspect can be interesting since the PHBH and PBAT have significantly different characteristics making them suitable for a wide range of applications. In fact, despite the growing interest in more sustainable materials for AM, the direct comparison of biodegradable polymers such as PHBH and PBAT in the context of FFF remains unexplored, especially the filament extrusion behaviour, the interlayer adhesion, and the final 3D-printed parts performances. This study can represent a comprehensive analysis of the thermal, viscoelastic, and mechanical properties of these two biopolymers starting from the filaments production. It also aims to investigate the printability of PHBH and PBAT via FFF. It can provide a preliminary study for researchers and industrial stakeholders on the comparison between the thermal and thermo-mechanical behavior of the biopolymers as greener alternatives for FFF 3D printing solutions, by filling the gap present right now in the literature.

2 Materials, equipment, and characterization testing

2.1 Materials

PHBH and PBAT were provided in form of pellets by MAIP Group (MAIP srl, Settimo Torinese, Torino, Italy). PHBH is a co-polymer characterized by melt flow index (MFI) of 3 g/10 min (170 °C, 5 kg) and density of 1.22 g/cm^3, whereas PBAT has MFI of 5 g/10 min (190 °C, 2.16 kg) and density of 1.26 g/cm^3, as reported in the supplier datasheets.

2.2 Manufacturing of filaments

The starting biopolymers, PHBH and PBAT, in form of granules were first dried in an oven at 80 °C for 24 h and characterized by means of thermogravimetric (TG) and differential scanning calorimetry (DSC) analyses. Then, two different filaments were produced using the Precision 350 extruder machine provided by 3Devo B.V (Atoomweg, Utrecht, Netherlands). The extruder presents a die (nozzle) with a diameter of 4 mm. The die had a circular cross-section with a diameter of 1.75 mm, matching the target filament diameter. There is a single extrusion screw inside the extruder barrel made of a nitride high-chromium and molybdenum steel alloy with a length of about 335 mm. The output filament diameter that the machine can produce is in the range from 0.5 mm to 3.0 mm.

The extruder is equipped with four thermocouples, *T*1, *T*2, *T*3, and *T*4, measuring the temperature at different points along the extruder barrel: *T*1 indicates the feed zone; *T*2 is the compression zone; *T*3 refers to the metering zone; and *T*4 is the die exit temperature, as summarized in Table 1. The cooling zone immediately after the die showed an effective cooling length of approximately 150 mm, ensuring controlled solidification of the extruded filament. Another important parameter to set for good filament extrusion was the screw extruder speed, set at 5 r/min for producing high-quality, diameter-stable filament because it reduces shear heating, improves melt quality, and avoids mechanical overload. The produced filaments were cooled using an air flow coming from a cooling fan to preserve their dimensional accuracy. The filaments diameter was continuously monitored in-line using the extruder's integrated laser diameter measurement system to monitor filament dimensions continuously during extrusion. The main extrusion parameters, which were optimized through a trial-and-error approach, are shown in Table 1.

Both PHBH and PBAT filaments were dried before to proceed with the printing process via FFF to remove moisture, which could negatively affect printability and thermal properties. Filaments were dried in an oven at 80 °C for 12 h, and then stored in a desiccator until use.

Table 1 Process parameters used to extrude PHBH and PBAT filaments

Sample	Thermocouple temperature/°C				Screw extruder speed/(r·min^{-1})
	*T*1 feed zone	*T*2 compression zone	*T*3 metering zone	*T*4 die temperature	
PHBH	145	145	140	125	5
PBAT	135	135	130	115	5

2.3 Manufacturing of 3D-printed parts

Specimens were fabricated via an FFF 3D printer (Anycubic Kobra Neo 2 machine provided by Shenzhen Anycubic Technology Co, Ltd., Shenzhen, Guangdong, China) with PHBH and PBAT utilized as thermoplastic biopolymer filaments.

The printing parameters were optimized to ensure stable processability and satisfactory part quality for both filaments produced. The optimization focused on identifying parameter combinations that enabled continuous material extrusion, good interlayer adhesion, dimensional accuracy, and surface quality, while avoiding typical printing defects. A set of key printing parameters was selected for optimization, including nozzle temperature, build plate temperature, printing speed, layer height, and cooling conditions. The parameter ranges were chosen based on preliminary trials and material-specific processability considerations and adjusted iteratively while printing standard test geometries. Typical defects observed during initial trials included under-extrusion, poor layer bonding, surface roughness, and edge deformation. These defects were mitigated by adjusting nozzle temperature and printing speed to improve melt flow, optimizing cooling conditions, and fine-tuning build plate temperature to enhance adhesion.

PHBH is a microbial polyester whose molecular chains are made naturally by bacteria as part of their metabolism. It is biosynthesized inside microbial cells. Its ester-based molecular structure makes the polymer more heat-sensitive, and more prone to thermal degradation, requiring controlled processing temperatures. For this reason, an extrusion temperature of 200 °C was chosen after several attempts to avoid thermal degradation according to the results of TGA and DSC performed on the pellets. While this temperature supports partial melting and layer fusion, it may risk insufficient viscosity reduction if the heating profile is not optimized [47]. The selected temperature is therefore a compromise between avoiding degradation and achieving good level of printability. Moreover, a build plate temperature of 50 °C was employed to maintain the lower layers above their glass transition temperature and reduce the generation of internal

stresses during the cooling considering that PHBH, being more crystalline, is prone to warping phenomenon.

Literature suggests that elevated build plate temperatures can help to mitigate the deformation in PHAs materials, like PHBH [48]. The selected extruder temperature for PBAT was 185 °C, which was within the optimal processing range (180–220 °C) ensuring an adequate melt flow and an interlayer diffusion without inducing thermal degradation. Considering these aspects, the build-plate temperature of 50 °C for PHBH is well below its crystallization and melting temperatures, and therefore it limits cold crystallization during printing. At this temperature, the material remains above its glass transition range but below the temperature, where crystallization kinetics become pronounced. Because of this, the crystallinity gradient between the bottom and top layers is expected to be minimal.

For PBAT, the build-plate temperature of 75 °C was selected experimentally to ensure reliable first-layer adhesion while preventing excessive softening or deformation. PBAT exhibits relatively low crystallinity and has a broad softening range; therefore, mild heating is beneficial for reducing warpage and internal stresses. The results showed that 75 °C provided stable adhesion among layers without causing thermal distortion of the initial layers. In fact, PBAT has good thermal stability, and it is known to retain its mechanical properties under these conditions [49]. In this case, a build plate temperature of 75 °C was sufficient to support a good adhesion without excessive softening of the first layer. PBAT has also relatively low crystallinity and benefits from mild bed heating to minimize shrinkage-related warping. In both the cases, the print speed was maintained at 50 mm/s with a layer height of 0.2 mm. Moreover, the 3D-printed samples were produced by depositing successive layers with different orientations, one at +45° and the other at − 45° for the whole printing process, and an infill of 100%. A trial-and-error method was employed to optimize the FFF process parameters reported in Table 2 for both the polymers investigated, and then successfully used to fabricate the 3D-printed specimens.

A schematic diagram illustrating the complete processing route, from granulates to extrusion, filaments production, and final FFF-printed parts, is shown in Fig. 1, providing a clear visual overview of the workflow and facilitating understanding of the experimental procedures.

Table 2 Process parameters of 3D-printed via FFF of PHBH and PBAT

Printing parameter	PHBH	PBAT
Extruder temperature/°C	200	185
Build plate temperature/°C	50	75
Print speed/(mm·s^{-1})	50	50
Fan cooling speed/(r·min^{-1})	1 050	1 050
Glue	Yes	No
Layer height/mm	0.2	0.2
Infill/%	100	100
Infill orientation (*x*/*y*)/(°)	− 45/+45	− 45/+45

2.4 Characterization techniques

Thermogravimetric analysis (TGA) was carried out using a Mettler-Toledo TGA 851e Instrument (Columbus, OH, USA) from 25 °C to 800 °C in air with a flow of 50 mL/min and a heating rate of 10 °C/min. Three measurements for each sample were performed.

DSC was carried out using a Netzsch 214 Polyma Equipment (Selb, Germany) from − 50 °C to 200 °C in nitrogen atmosphere with a flow of 40 mL/min and a heating/cooling ramp of 10 °C/min. Three measurements for each sample were performed. A first heating cycle was used to erase the thermal history of the samples. Then, a cooling cycle and a second heating were recorded and used to evaluate the thermal transitions of PHBH and PBAT. From DSC measurements, it has been possible to determine the melting and crystallization temperatures (T_m and T_c) and the glass transition temperatures (T_g) of the two biopolymers. The midpoint of the total change in heat

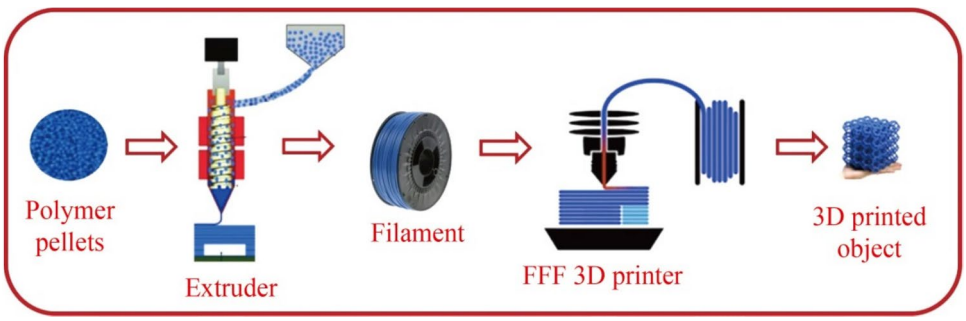


Fig. 1 Schematic representation of the processing for PHBH and PBAT: granulate → extrusion → filament → 3D printing via FFF→ printed specimens

capacity was designated as the T_g and the peak temperatures as the melting and crystallization point. Moreover, the crystallization degree (X_c) of the two biopolymers were evaluated by using Eq. (1)

$$X_c = \frac{\Delta H_m - \Delta H_{cc}}{\Delta H_m^0} \times 100\ \%\ , \tag{1}$$

where ΔH_m is the melting enthalpy and ΔH_{cc} is the cold crystallization enthalpy, both determined from the cooling and second heating cycle of the DSC measurements. ΔH_m^0 is the melting enthalpy of the fully crystalline polymers, i.e., 115 J/g for PHBH [50], and 114 J/g for PBAT [51].

Dynamic-mechanical analysis (DMA) was carried out according to ASTM D4065 at a frequency of 1 Hz from 0 °C to 200 °C using an Anton Paar MCR 702e Multi Drive Rheometer (Graz, Austria) in tensile configuration. Three rectangular 3D-printed specimens with 50 mm in length, 10 mm in width, and 2 mm in thickness were tested.

Tensile testing was conducted to assess both the mechanical strength and stiffness of the materials. These tests were carried out following the ISO 527-2 standard for polymer specimens using an Instron® 5989 universal testing machine, fitted with a 1 kN load cell. To determine the elastic modulus, an Instron 2620-61 extensometer with a 12.5 mm gauge length was employed. For each material type, six dog-bone specimens were analyzed within a strain range of 0–0.3%, and the elastic modulus (E) was calculated using the "chord modulus" method between strain values of 0.05% and 0.25%. The elastic tests were performed at a constant strain rate of 0.025 min^{-1}. To measure the ultimate tensile strength (UTS) and elogation at break (ε_b), separate tensile tests were conducted at a crosshead speed of 5 mm/min. This tensile test speed was selected based on standard testing practices for thermoplastic polymers and previous literature on PHBH and PBAT [52, 53]. This rate provides a balance between minimizing strain-rate effects and ensuring accurate measurement of mechanical properties, such as elastic modulus and ultimate tensile strength, for both filaments and printed specimens. This speed allows reliable comparison between the two biopolymers under consistent testing conditions. All tests were carried out under controlled environmental conditions, with temperature maintained at 20 °C and relative humidity at 50%.

Optical microscopy observations were performed using a Leica DMI 5000 M optical microscope (Leica Microsystems, Germany) to qualitatively evaluate the surface morphology and microstructural features of the printed samples, allowing the identification of defects, layers adhesion, and processing-induced heterogeneities.

3 Characterization of PHBH and PBAT biopolymers

3.1 Characterization of pellets

Before processing PHBH and PBAT pellets, TGA and DSC measurements were carried out to study the thermal degradation behaviour and the thermal transitions of the pristine materials to have preliminary indications about their processability through filament extruder.

Figures 2 and 3 show the thermogravimetric curves performed in air and their first derivatives for the two biopolymers under investigation, PHBH and PBAT, respectively. For clarity, the materials were labelled according to their processing stage: PHBH_p and PBAT_p refer to the pellets, PHBH_f and PBAT_f to the extruded filaments, and PHBH_3D and PBAT_3D for the specimens manufactured by FFF. From the TGA of Fig. 2 performed on the PHBH pellets in oxidant atmosphere, it is possible to see that it

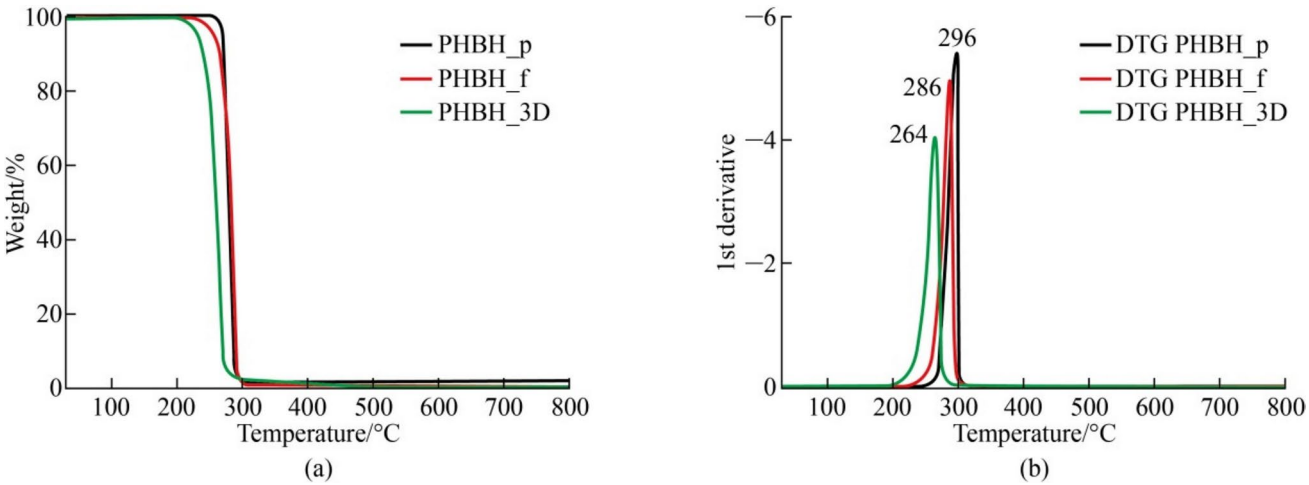


Fig. 2 TG and DTG curves of PHBH: pellet, filament, and printed

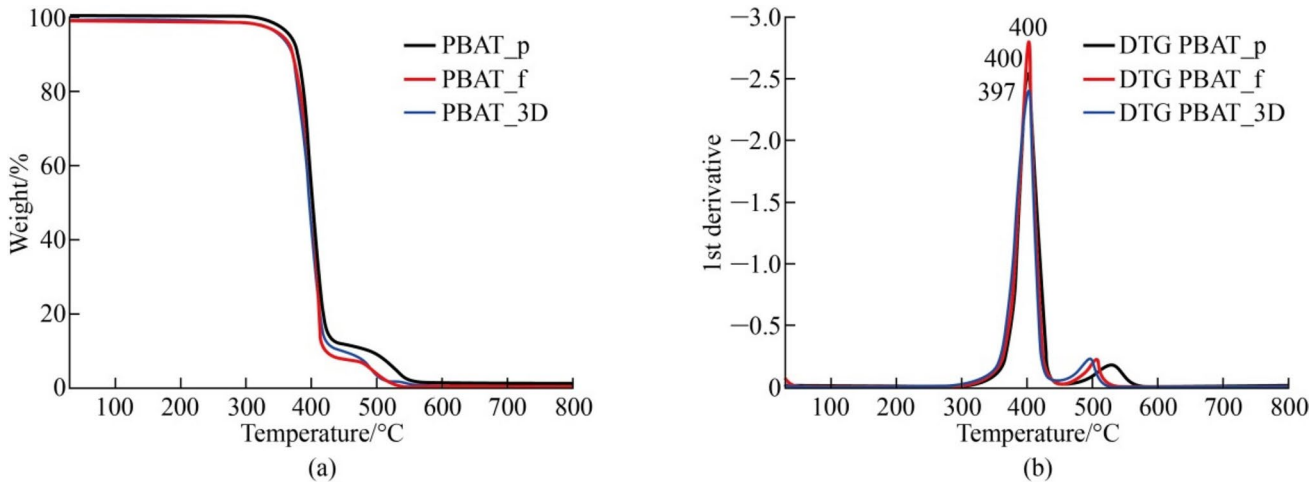


Fig. 3 **a** TG and **b** DTG curves of PBAT samples: pellet, filament, and printed

Table 3 Thermal data determined by TGA performed in air and DTG curves of PHBH and PBAT in the form of pellets, filaments, and printed samples

Sample	T_{onset}/°C	T_{50}/°C	$T_{max\ deg}$/°C
PHBH_p	268	277	296
PHBH_f	256	282	286
PHBH_3D	231	260	264
PBAT_p	363	400	400
PBAT_f	356	398	400
PBAT_3D	354	397	397

starts to degrade at 274 °C, by means of a single main degradation step showing the maximum peak at 296 °C due to the chain scission of the ester bonds [32]. No ash is noted at the end of the analysis at 800 °C.

Differently, PBAT presents a degradation behaviour consisting of two main peaks with the maxima at 400 °C and 527 °C. The first peak is related to the aliphatic segment's degradation, like the butylene adipate units, which tend to breakdown at lower temperatures because they are less thermally stable. The second peak at higher temperature can be associated to the degradation of the terephthalate units, which have higher thermal stability due to the aromatic rings [32]. An ash content of zero is found in this case at the end of the measurement, as also visible from the data of Table 3.

The DSC analyses were also carried out to determine the thermal transitions of the two biopolymers, and evaluate how the melting/crystallization behaviour could affect the extrusion parameters, in terms of temperature and speed. This enables us to optimize the extrusion temperature profile, avoid the polymer degradation, and achieve a filament of good quality. Figure 4 shows the DSC curves of the PHBH specimens.

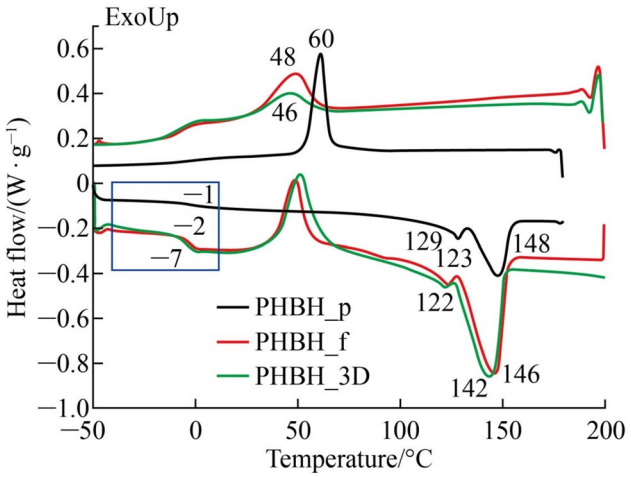


Fig. 4 DSC curves PHBH samples: pellet, filament, and printed via FFF

The DSC analysis shows that by increasing the temperature from − 50 °C up to 200 °C, PHBH presents a small glass transition visible at − 1 °C and two distinct endotherm peaks at 129 °C and 148 °C, reflecting the melting of different crystalline regions [50]. During the cooling scan, PHBH shows a single exothermic peak corresponding to the temperature of crystallization (T_c). By analysing the enthalpy associated with the melting of the biopolymer, it was also possible to estimate the degree of crystallization, according to Eq. (1). The degree of crystallization of the PHBH pellets was estimated to be 44%. All DSC data, obtained analysing PHBH pellets, filaments, and 3D-printed parts, are summarized in Table 4.

Figure 5 shows the DSC curves of the PBAT in the form of pellet, filament, and printed samples.

Table 4 Thermal properties of PHBH determined by DSC in nitrogen

Sample	T_m/°C	T_g/°C	ΔH_m/(J·g^{-1})	T_c/°C	ΔH_{cc}/(J·g^{-1})	X_c/%
PHBH_p	129/148	−1	50.60	60	–	44
PHBH_f	123/146	−2	56.84	48	25.12	28
PHBH_3D	122/142	−7	48.65	46	33.56	13

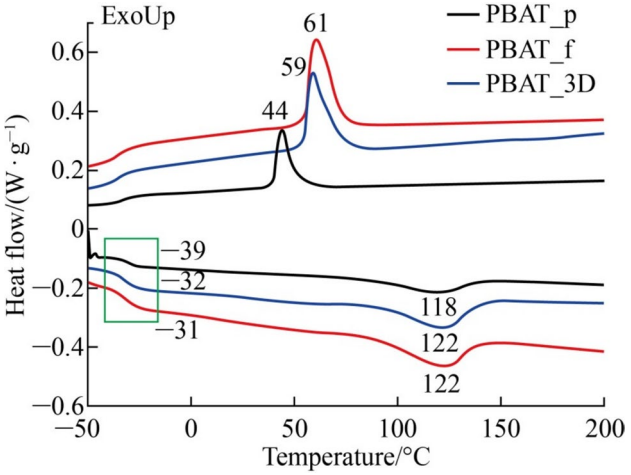


Fig. 5 DSC curves PBAT samples: pellets, filament, and printed via FFF

The cooling cycle also reveals the presence of a well-defined exothermic peak representing the temperature at which the polymer chains start organizing into crystalline regions. The T_c is found at 44 °C and it plays an important role for the PBAT processing. The crystallization degree for PBAT calculated is around 15% to underline that PBAT, as semi-crystalline polymer, has a relatively low degree of crystallinity due to its copolymer structure and the presence of flexible segments, as previously shown in Ref. [51]. Table 5 reports the DSC values for PBAT in the form of pellet, filament, and printed samples.

3.2 Characterization of filaments

PHBH and PBAT pellets were extruded into filaments via melt extrusion using a single-screw laboratory-scale extruder with optimized temperature profiles to prevent premature thermal degradation and achieve uniform filament diameter, as close as possible to 1.75 mm for both the biopolymers. The filament fabrication starting from these materials can present challenges due to their thermal behavior, rheology, and mechanical properties. To monitor and control the filament diameter distribution, we directly evaluated the diameter tolerance during the extrusion by using an inline sensor, enabling it to provide real-time data, take multiple measurements around the filament's circumference, maintain consistent filament quality, and calculate the average diameters and their relative standard deviation. The resulting mean and standard deviations were calculated for statistical consistency. The filaments' diameter was measured to ensure consistency, print quality, and extrusion performance for the future FFF printing process, where the target diameter for optimal use was set to be (1.75±0.05) mm [54]. Table 6 shows the statistical results obtained for PHBH and PBAT filaments obtained via extrusion.

Comparing the results obtained for the two different biopolymers, it is possible to see that PHBH filament shows more frequent variations probably due to its sensitivity to thermal and shear conditions. The surface quality was generally smoother for PBAT filaments. While PHBH exhibits the tendency to become brittle upon cooling, PBAT retains flexibility, making it more suitable for spool handling and feeding in the FFF 3D printer. The filament produced using PHBH granules shows an average diameter of (1.80±0.05) mm revealing slightly more variability with minor inconsistencies with respect to the standard specification (1.75 mm) probably due to the elastic deformation post-die [55, 56]. Whereas the second filament produced using PBAT shows a more regular diameter with an average of (1.74±0.04) mm, which remains as close as possible to the standard 1.75 mm value for FFF.

Table 6 Statistical data of the PHBH and PBAT filaments production via extrusion

Sample	Average/mm	Median/mm	Std Dev/mm	Max/mm	Min/mm
PHBH	1.80	1.80	0.05	1.91	1.60
PBAT	1.74	1.75	0.04	1.97	1.50

Table 5 Thermal properties of PBAT determined by DSC in nitrogen

Sample	T_m/°C	T_g/°C	ΔH_m/(J·g^{-1})	T_c/°C	X_c/%
PBAT_p	118	−39	17.50	44	15
PBAT_f	122	−31	17.12	61	15
PBAT_3D	122	−32	14.87	59	13

These measurements clearly indicate a general consistent extrusion process for both the biopolymers with tolerances suitable for standard 3D printing applications via FFF. The slight variation observed for PHBH falls within acceptable limits, though it suggests the need for careful control of the extrusion temperature and puller speed, as PHBH is more sensitive to thermal degradation and flow instability, as already shown in Ref. [57]. The observed consistency in filament diameter for PBAT reflects its favorable processing behavior, particularly its thermal stability and elasticity. These minor fluctuations can be attributed to the elastic deformation occurring during the post-extrusion cooling, a well-known behavior in PBAT-based filaments [56]. These results suggest that PBAT can be reliably processed into filament form with minimal deviation from FFF requirements.

The thermal properties of the two produced thermoplastic filaments were also investigated by means of TGA and DSC analyses to understand if the thermal characteristics of the biodegradable materials were altered during the extrusion process, which helps to select the optimal printing process parameters via FFF. The TGA and DSC curves of the two filaments fabricated via extrusion are shown in Figs. 2, 4 for PHBH and Figs. 3, 5 for PBAT filaments respectively. Looking at the TG and DTG curves in Fig. 2, which are representative of the PHBH filament, it can be seen that the polymer in the form of filament begins to degrade at 256 °C and decomposes in a single step, with the maximum degradation temperature peaking at 286 °C, 10 °C lower than that of the corresponding PHBH pellet (see Table 3). This can be probably due to the high sensitivity of the biopolymer to thermal degradation during the extrusion process [57]. The filament, produced starting from PBAT pellets, shows two main degradation steps corresponding to the breakdown of the butylene adipate units at 400 °C, followed by the degradation of the aromatic terephthalate units at 514 °C. The slight 13 °C temperature shift of the second degradation peak is indicative of minor changes in the thermal behaviour of the polymer, including its crystallization that occur during the extrusion processing [58].

This result was confirmed by DSC analyses performed in nitrogen on the two different biopolymers, as reported in Fig. 4 for PHBH and Fig. 5 for PBAT, respectively. The DSC curves of the PHBH filament clearly indicate that the filament production via extrusion led to a slight shift of T_m values towards lower temperatures depending on molecular weight changes due to thermal degradation occurring during the extrusion, as visible from the data of Table 3. Moreover, it is possible to observe the presence of an exothermic peak at 48 °C due to tendency of the semi-crystalline polymer to crystallize during the second heating cycle before to melt, producing a cold crystallization peak due to the crystallization of amorphous regions, as already seen for the pellets. A decrease of T_c value from 60 °C for the pellet to 48 °C for the filament is also accompanied by a significant decrease of the degree of crystallinity from 44% to 28%, as reported in Table 4.

This behaviour can be caused by a fast-cooling rate during the filament formation, which can negatively affect the crystallinity. On the contrary, for PBAT it is possible to observe from the DSC curves of Fig. 5 that the T_m remains generally stable while there is an increase in the T_c value from 44 °C to 61 °C to underline that extrusion can significantly alter the molecular orientation of PBAT and often induce the polymeric chains alignment. The crystallinity remains unchanged at 15%. PBAT also shows a slight reduction of the T_g value from − 39 °C for the pellet to − 31 °C for the filament because the new orientation can restrict the chain mobility, requiring more thermal energy to reach the glass transition. The DSC results of PBAT filament are reported in Table 5.

3.3 Characterization of printed samples

The two filaments obtained via extrusion using PHBH and PBAT were successfully employed to fabricate several 3D-printed parts via FFF, starting from simple geometries such as rectangular bars and dog-bone-shaped specimens, which were mainly used to set the optimal printing parameters and for the characterization, up to the fabrication of more complex structures.

The rectangular bars were used to compare the effect of the printing process within the FFF 3D printer on the PHBH and PBAT thermal and viscoelastic properties. The dog-bone specimens were tested to assess the differences of the mechanical behaviours of the two different biopolymers. By comparing the TG curves of the filaments and the printed parts of Fig. 1, it is possible to observe that the red and blue curves have the same behaviour indicating that the printing process performed via FFF does not have significant effect on the thermal stability of PHBH. The main degradation peaks are centred at 286 °C for the PHBH-based samples and 397 °C for the PBAT-based ones, which are almost superimposable on the maximum peaks of degradation temperatures of the filaments.

All TGA data collected in Table 3 reveal a progressive decrease in the thermal stability of PHBH as the material undergoes filament extrusion and subsequent 3D printing. PHBH pellets exhibit the highest thermal stability, with an onset degradation temperature (T_{onset}) of 268 °C. After filament extrusion, T_{onset} decreases to 256 °C, indicating moderate thermal degradation induced by melt processing. A more pronounced reduction in thermal stability is observed for the 3D-printed samples, which show a T_{onset} of 231 °C. This behaviour suggests cumulative thermo-mechanical degradation during the multiple heating cycles associated

with filament extrusion and fused filament fabrication. The decrease in T_{onset} and $T_{max\ deg}$ is consistent with chain scission phenomena, leading to reduced molecular weight and lower resistance to thermal degradation, as already reported in Ref. [57]. Moreover, all samples display a single main degradation step and negligible residue at 800 °C, confirming the absence of inorganic fillers or thermally stable additives and indicating that degradation proceeds primarily through volatilization of organic components. Despite the observed decrease in thermal stability, the degradation onset temperatures remain well above the printing temperature range, confirming the suitability of PHBH for fused filament fabrication under controlled conditions [57]. In contrast, PBAT exhibits considerably higher thermal stability than PHBH, with onset degradation temperatures of 363 °C, 356 °C, and 354 °C for pellets, filament, and 3D-printed states, respectively. The corresponding maximum degradation temperature values remain close to 400 °C across all processing states. PBAT has higher thermal stability than PHBH and is less sensitive to filament extrusion and 3D printing reflecting superior resistance to processing-induced thermo-mechanical degradation. This larger thermal window makes it more robust to variations in processing parameters, which is consistent with previous findings [58].

Furthermore, some effects of the printing processing on the PHBH and PBAT are visible on the thermal transitions of the printed specimens of the two biopolymers, as evident from the DSC curves of Fig. 4 for PHBH and Fig. 5 for PBAT, respectively.

Looking at the green DSC curves of the PHBH-based samples shown in Fig. 4, it is possible to observe that T_m and T_c are located at almost the same temperature as those of the filament. On the contrary, the DSC thermogram acquired during the second heating reveals a slight decrease of the T_g value from − 2 °C to − 7 °C and the appearance of a cold crystallization peak located at 50 °C, which clearly indicates that PHBH is not fully crystallized during the cooling phase of the FFF process. This means that the crystallization is incomplete during the printing process with residual amorphous regions crystallizing upon reheating giving rise to a cold crystallization phenomenon [56]. The polymer chains did not arrange themselves into a fully crystalline structure during the printing process, probably due to fast cooling after extrusion, insufficient time for crystalline domains to form, or the molecular mobility being too low, as also suggested by the decrease in T_g. This implies that a significant fraction of the polymer remained in the amorphous state after extrusion. This finding was also confirmed by the significant reduction in the degree of crystallization, which shifted from 28% for the PHBH filament before the printing to 13% for the sample printed via FFF, as reported in Table 4.

The DSC thermogram of the PBAT-based specimens reported in Fig. 5 (see blue curve) does not show significative changes with respect to the heating and cooling curves of the filament. This result suggests that the PBAT can crystallize during the cooling phase of the FFF process. Unlike PHBH, PBAT has probably enough time and mobility to form fully crystalline regions. As a result, PBAT reaches a higher degree of crystallinity during printing, reducing the need for further structural rearrangement upon thermal analysis, as shown in Table 4. In this case, the degree of crystallinity of the biopolymer remains almost the same before and after the printing process (15%–13%).

3.4 Thermo-mechanical and mechanical properties of 3D-printed parts realized via FFF

The viscoelastic properties of the 3D-printed samples obtained via FFF using PHBH and PBAT biopolymers were also determined by means of DMA analyses to have indication about their storage modulus and estimate the glass transition temperature as the maximum of tanδ curves in function of the increasing temperature. Figure 6 presents the plots of the extensional storage moduli and tanδ curves for PHBH and PBAT.

The results obtained from DMA evaluated at 25 °C clearly indicate that the PHBH-based specimens tend to be more rigid (E'= 1 037 MPa) due to its semi-crystalline nature and relatively high glass transition temperature (14 °C) compared with the PBAT-based samples which are more flexible and ductile with a value of storage modulus of 56 MPa.

In fact, PBAT has a much lower T_g (− 25 °C), so it is already in a rubbery state at room temperature, and this confers it greater flexibility and elongation under stress with respect to PHBH. Instead, once above T_g, PHBH rapidly loses stiffness and becomes much more compliant. Table 7 shows the tanδ values and the extensional storage and loss moduli of the rectangular samples obtained by FFF using the two biopolymers. As well-known from literature, the glass transition temperature of PHBH and PBAT differs depending on the measurement technique due to the different physical phenomena probed by DSC and DMA [59, 60]. The lower T_g obtained by DSC (− 7 °C for PHBH and − 32 °C for PBAT) reflects the calorimetric glass transition due to changes in heat capacity, associated with the onset of cooperative segmental mobility in the amorphous phase under quasi-static thermal conditions. The higher T_g measured by DMA (14 °C for PHBH and − 25 °C for PBAT) corresponds to the onset of mechanical softening under dynamic loading. In fact, DMA measures T_g as the temperature at which a pronounced decrease in storage modulus and a peak in tanδ are observed, reflecting the onset of mechanical relaxation under an applied oscillatory deformation. Because DMA probes

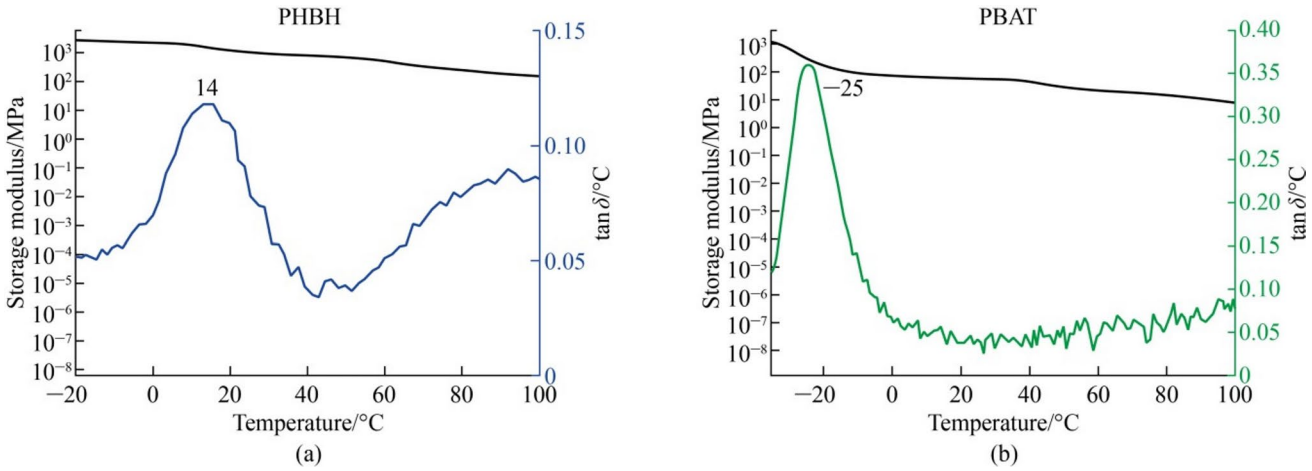


Fig. 6 DMA curves of **a** PHBH and **b** PBAT 3D-printed parts realized by FFF

Table 7 Viscoelastic properties of PHBH and PBAT 3D-printed specimens evaluated at 25 °C

Sample	Storage modulus/MPa	Loss modulus/MPa	$T_{\tan\delta\ \max}$/°C
PHBH	1 037	81	14
PBAT	56	2	−25

Table 8 Mechanical properties of PHBH and PBAT 3D-printed specimens

Sample	Elastic modulus/MPa	Ultimate tensile strength/MPa	Elongation at brake/%
PHBH	842 ± 99	12 ± 1	5.0 ± 0.5
PBAT	61 ± 10	11 ± 1	1 030 ± 101

time-dependent viscoelastic behaviour at a finite frequency, the apparent T_g is shifted to higher temperatures [59, 60]. Consequently, the storage moduli were evaluated at 25 °C, and these were significantly lower than the values in the glassy state but remained finite due to the presence of crystalline domains acting as physical crosslinks. The storage modulus values, measured for both the biopolymers at room temperature, reflect a balance between increased molecular mobility in the amorphous phase and reinforcement provided by the crystalline phase (see Table 7).

Since the service temperature exceeds T_g, detected from DMA, the storage modulus is governed primarily by viscoelastic chain dynamics rather than glassy stiffness, making it representative of the material's in-service load-bearing capability.

This trend was confirmed by the tensile properties of the 3D-printed specimens obtained via FFF evaluated by means of tensile testing. Table 8 listed the results obtained for PHBH and PBAT dog bone-shaped specimens.

PHBH shows a relatively stiff behaviour for a biodegradable polyester showing an elastic modulus of 842 MPa, a tensile strength of 12 MPa and a moderate elongation at break of 5.0%. PHBH exhibits good mechanical properties suitable for various industrial applications, as it typically has a high elastic modulus, making it more rigid and structurally stable under low loads [52]. Understanding these mechanical properties is crucial for selecting PHBH for specific applications, for example, structural components for applications requiring higher strength are not compatible with the PHBH tensile strength, which can represent a limiting factor [50]. A completely different mechanical behaviour can be observed for PBAT 3D-printed specimens. The elastic modulus value is very low, about 61 MPa, reflecting a very flexible material, while the elongation at break is higher than 1 000%, making PBAT very ductile and rubbery, as indicated in Table 8. These properties highlight PBAT's flexibility and ductility, making it suitable for applications requiring high flexibility and elongation [53]. This behaviour can be explained considering that during the extrusion process and the following 3D printing process via FFF, PBAT undergoes several changes in terms of reduction of molecular weight, thermal degradation, and crystallinity that potentially affect the final mechanical properties. These key factors can result in a low tensile strength and very high elongation at break [56].

3.5 3D-printed parts realized via FFF

Based on the findings coming from thermal and thermomechanical analyses, more complex parts were 3D-printed via FFF using the PHBH and PBAT filaments to realize demonstrators for possible applications in biomedical fields. Figure 7 displays different views of two different examples

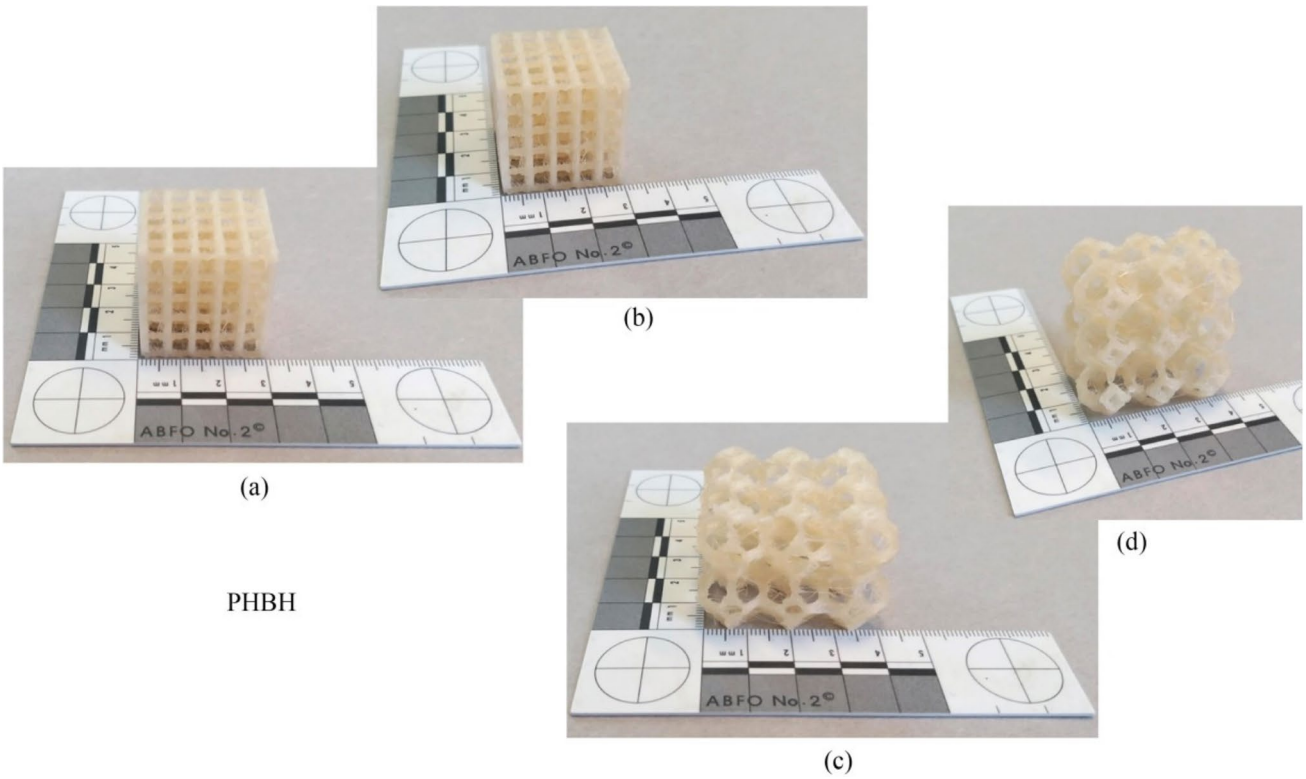


Fig. 7 Different views of two complex 3D-printed parts realized by FFF using PHBH

of printed specimens fabricated by FFF using PHBH as starting biopolymer. The pictures of Figs. 7a, b show a regular cubic-shaped lattice realized with 30 mm in *x*, *y*, and *z* printing directions, whereas Figs. 7c, d report the images of a strut-shaped structure characterized by an intricate internal pattern made of repetitive square unit cells. The dimensions for this designed component were 30 mm in *x* and *z* directions, and 20 mm in *y* direction.

The component exhibits little printing defects due to both intrinsic material properties and process parameters, such as a lower interlayer adhesion probably due to the semi-crystalline nature of PHBH, which can hinder the appropriate adhesion between two consecutive layers of polymer leading to delamination, as observed in some regions of the printed structure. These defects are clearly visible in the optical microscopy images of a PHBH complex lattice structure printed via FFF (see Fig. 8).

Observations via optical microscopy reveal semi-transparent films and thin polymer filaments spanning pores and lattice openings, especially within square cells and between struts; such morphologies are typical of inadequate melt retraction, low melt viscosity, and low melt rigidity, as illustrated in Figs. 8b, c. Surface thin membranes are typical in lattice structures close to overhangs without supports and bridging regions between two consecutive points. Such defects occur when the material in the molten state cannot adequately support its own weight or solidify fast enough probably due to insufficient retraction settings and the material's relatively low melt stiffness, resulting in the formation of little surface imperfections. Additionally, a detailed view of filament deposition revealing some minor surface irregularities is reported in Fig. 8d, while no significant interlayer delamination or macroscopic defects are evident, indicating an overall good print quality.

The same parts printed via FFF for PHBH were obtained by using the PBAT filament, as shown in Fig. 9. The cubic lattice of Figs. 9a, b and the strut-shaped structure illustrated in Figs. 9c, d evidence a very high printing resolution and dimensional accuracy considering their architectures very challenging to print. The smooth and well-bonded surface suggests that the layers of the PBAT-based specimens are strongly adhered to realize the lattice shapes.

In this case, the PBAT-based complex geometries realized via FFF present a higher surface definition and level of details, not evidencing the defects previously discussed for the PHBH-based lattice structures. Figure 10 represents a macroscopic view of the same lattice structure and some microscopic details.

The macroscopic geometry of the lattice is well preserved for PBAT, and the pores exhibit a regular shape with uniform dimensions. The magnified view of the lattice pores of Fig. 10b highlights a uniform cell morphology, well-defined

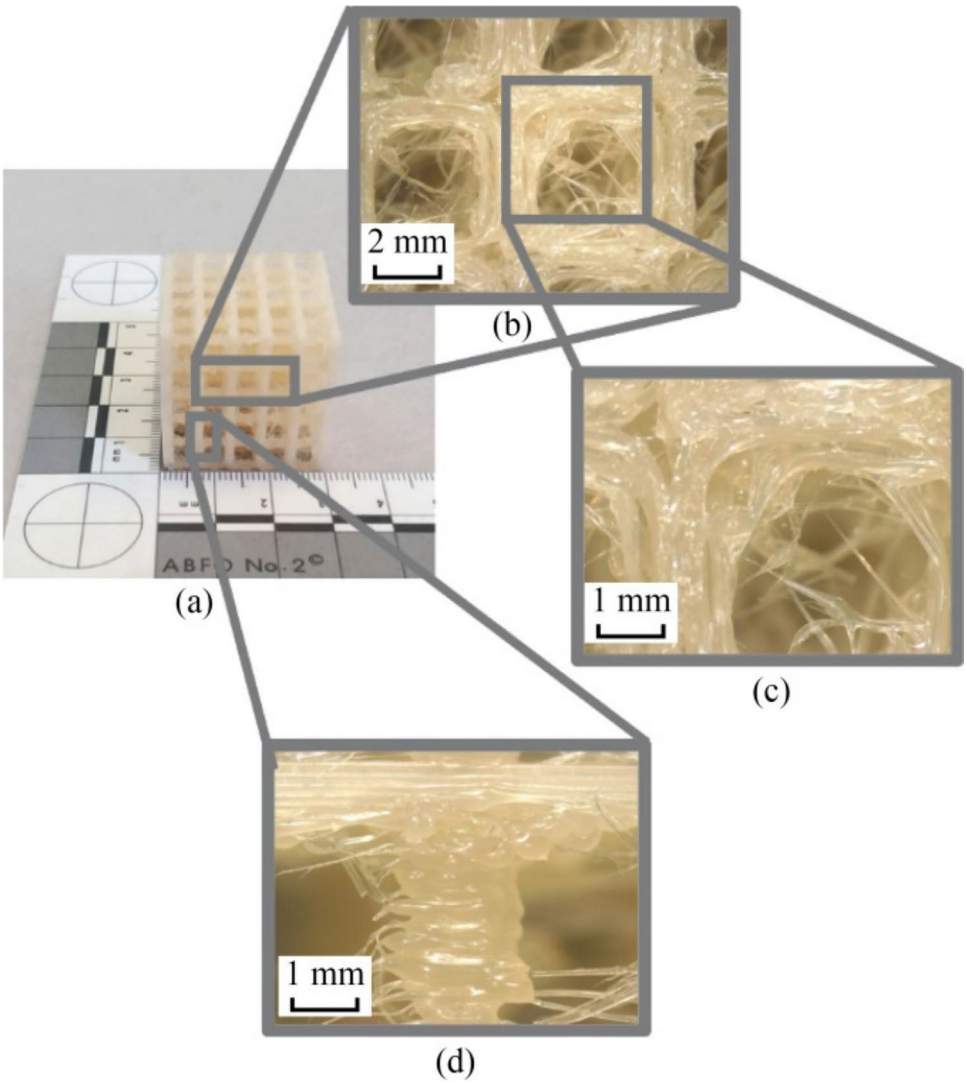


Fig. 8 **a** Macroscopic view of a PHBH printed lattice structure, **b** thin surface membranes and filament webbing, **c** stringing and bridging sagging between lattice struts, **d** detail of filament deposition and surface irregularities

cell structure, and more regular pore architecture. At higher magnification, limited filament stringing can be observed inside some lattice cells, appearing as thin polymer filaments spanning across the pores (see Fig. 10c). These features are localized in some points and do not significantly obstruct the pore openings. No pronounced interlayer delamination, pore collapse, or severe surface roughness is detected, indicating effective interlayer bonding and stable filament deposition during printing. The minor stringing observed can be likely related to melt flow behavior and retraction dynamics during deposition, but its limited extent suggests that the selected processing parameters are generally suitable for PBAT-based materials.

A comparative analysis of the printed components highlights distinct defect characteristics between PHBH and PBAT, primarily related to their different thermal behaviors. PHBH-based samples exhibit a higher tendency toward printing defects, including filament stringing, thin surface membranes in lattice pores, and occasional bridging sagging. These features can be mainly attributed to the semi-crystalline nature of PHBH, which can limit the interlayer adhesion and reduce melt strength during the deposition. In contrast, PBAT-based samples display overall smoother filament deposition and more regular lattice cells, with minor and localized filament stringing. No interlayer delamination or pore deformation is detected in PBAT prints, indicating a more stable melt behavior and effective layer bonding under the selected processing conditions. Overall, while both materials can be successfully processed via FFF using optimized printing parameters, PHBH shows a higher sensitivity to processing conditions that can be further improved,

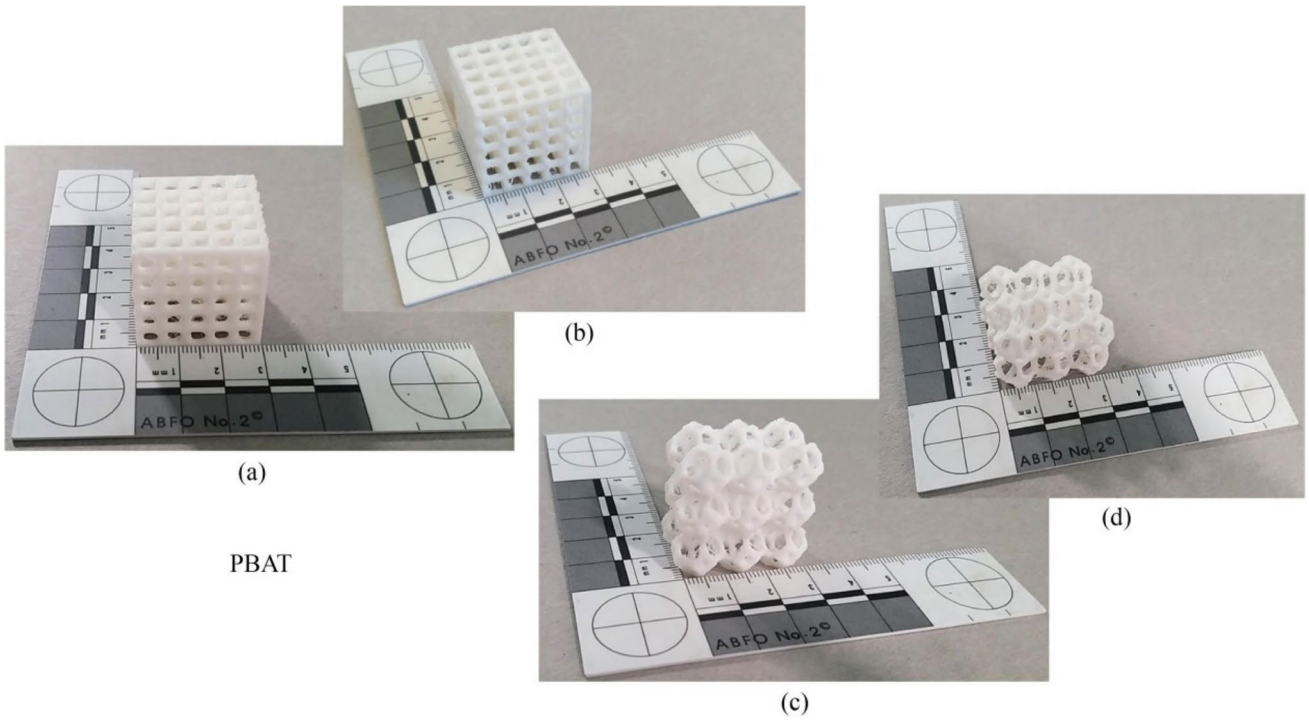


Fig. 9 Different views of two complex 3D-printed parts realized by FFF using PBAT

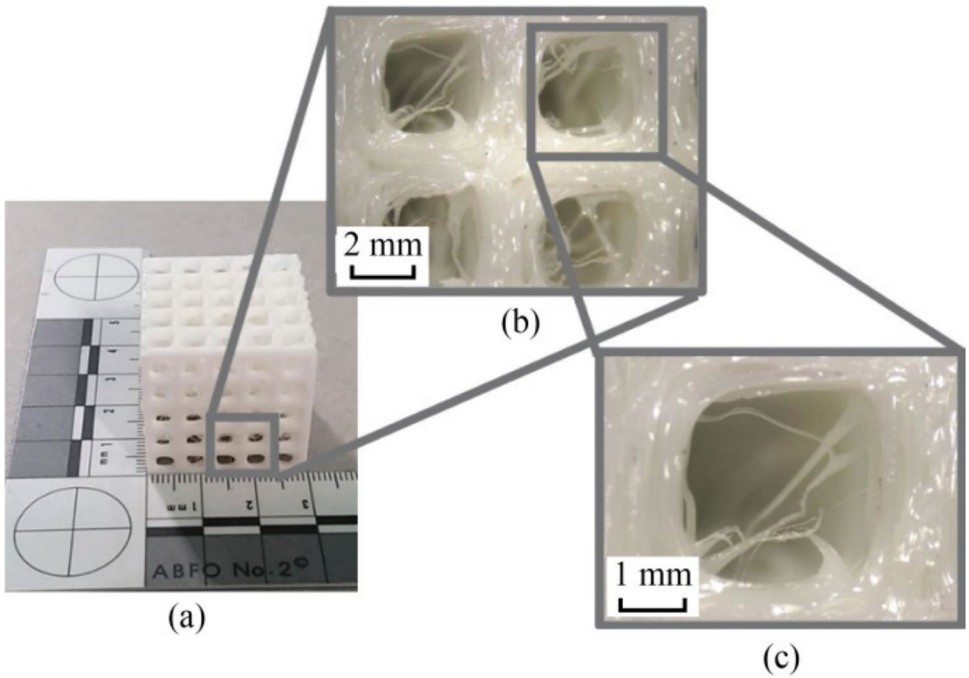


Fig. 10 **a** Macroscopic view of a PBAT printed lattice structure, **b** magnified view of lattice pore morphology, and **c** detail of minor filament stringing inside lattice cells

whereas PBAT demonstrates greater robustness in terms of print quality and defect minimization [56–58].

Moreover, the PBAT-based specimens are more flexible with respect to the previous ones, underlining the

great difference between the two biopolymers in terms of mechanical performances due to their completely different chemical compositions. These complex geometries could be printed via FFF and suggested for possible applications in the biomedical field as eco-friendly choices for tissue engineering and implantable devices and scaffolds due to the biocompatibility and biodegradability of the two biopolymers investigated. However, the PHBH printed lattice structures seem to be better suited to provide higher mechanical support for scaffold applications, as their rigidity is greater than that of PBAT, which in contrast, fits applications where high flexibility is strictly required.

4 Conclusions

This work systematically evaluated the thermal and thermo-mechanical behaviour of PHBH and PBAT biopolymers across all the main stages of an FFF processing, from the characterization of the commercial pellets to extruded filaments production up to the 3D-printed parts realization.

The dimensional analysis of the extruded filaments confirms that both biopolymers can be successfully processed into filaments with small diameter tolerances, ensuring reliable feeding and good print quality for FFF printing systems. The statistical consistency of both filaments' diameters, coupled with the successful fabrication of standardized test specimens and more complex geometries, underlines the good processability of both biopolymers using extrusion and FFF equipment. Several printed specimens were realized via FFF after optimization of the printing parameters. The results demonstrate that both PHBH and PBAT can be successfully processed from pellets to printed parts via FFF, even if each stage of processing induces predictable changes to their thermal behaviour and, consequently, of their mechanical properties. PHBH's thermal stability decreases progressively from pellet to filament extrusion up to 3D printing, as evidenced by the reduction in degradation temperature of around 30 °C. This trend is accompanied by a stable melting peak and decrease of crystallinity degree during the different phases. PHBH retains high stiffness and strength but remains brittle, limiting its use to applications where rigidity is prioritized over flexibility. In contrast, PBAT maintains high thermal stability throughout processing, with only minor reductions in degradation onset and melting peak temperature values. The mechanical profile of PBAT, with low elastic modulus, moderate strength, and very high elongation at break, makes it ideal for applications requiring high flexibility, such as soft components for biomedical field or packaging. Mechanical testing of FFF dog-bone 3D-printed specimens highlighted the contrasting mechanical profiles of the two biopolymers. PHBH demonstrated a high elastic modulus (842 MPa) and modest tensile strength (12 MPa), but limited ductility (5% elongation at break), consistent with its semicrystalline structure and higher degree of crystallinity. PBAT, on the other hand, exhibited a much lower elastic modulus (61 MPa) but exceptional ductility (1 030% elongation at break), with a tensile strength (11 MPa) comparable to PHBH. These findings highlight that PHBH offers higher stiffness and strength, with stable crystallinity and melting behaviour through processing, but its thermal stability decreases after extrusion and printing. On the contrary, PBAT exhibits superior thermal stability and exceptional ductility in the printed state, despite a notable reduction in crystallinity during filament extrusion. Its mechanical flexibility and moderate strength make it suitable for applications where flexibility is strictly required. However, both biopolymers can be reliably processed into filaments with low dimensional variability, supporting their proficiently application in FFF 3D printing technology.

Overall, the study provides a clear comparative framework for selecting PHBH or PBAT based on the required balance of stiffness, strength, and ductility in FFF printed components. The detailed thermal and thermo-mechanical characterization offers valuable guidance for optimizing process parameters and predicting end-use performance of PHBH and PBAT at each processing step, from pellets to printed specimens enabling an exhaustive understanding of how processing can influence the material final properties and, as result, their possible industrial applications.

Acknowledgements This study was carried out within the Materials sUSTainability for polymer Additive manufacturiNG (MUSTANG) project—funded by European Union—Next Generation EU within the PRIN 2022 program (D.D. 104-02/02/2022 Ministero dell'Università e della Ricerca). This manuscript reflects only the authors' views and opinions. The Ministry cannot be considered responsible for them.

Funding Open access funding provided by Politecnico di Torino within the CRUI-CARE Agreement.

Open Access This article is licensed under a Creative Commons Attribution 4.0 International License, which permits use, sharing, adaptation, distribution and reproduction in any medium or format, as long as you give appropriate credit to the original author(s) and the source, provide a link to the Creative Commons licence, and indicate if changes were made. The images or other third party material in this article are included in the article's Creative Commons licence, unless indicated otherwise in a credit line to the material. If material is not included in the article's Creative Commons licence and your intended use is not permitted by statutory regulation or exceeds the permitted use, you will need to obtain permission directly from the copyright holder. To view a copy of this licence, visit http://creativecommons.org/licenses/by/4.0/.

References

1. Abdulhameed O, Al-Ahmari A, Ameen W et al (2019) Additive manufacturing: challenges, trends, and applications. Adv Mech Eng 11(2):1–27. https://doi.org/10.1177/1687814018822880

2. Sun C, Wang Y, McMurtrey MD et al (2021) Additive manufacturing for energy: a review. Appl Energy 282:116041. https://doi.org/10.1016/j.apenergy.2020.116041
3. Rasiya G, Shukla A, Saran K (2021) Additive manufacturing—a review. Mater Today Proc 47:6896–6901. https://doi.org/10.1016/j.matpr.2021.05.181
4. Pelzer L, Hopmann C (2021) Additive manufacturing of non-planar layers with variable layer height. Addit Manuf 37:101697. https://doi.org/10.1016/j.addma.2020.101697
5. Bose S, Ke D, Sahasrabudhe H et al (2018) Additive manufacturing of biomaterials. Prog Mater Sci 93:45–111. https://doi.org/10.1016/j.pmatsci.2017.08.003
6. Bahnini I, Rivette M, Rechia A et al (2018) Additive manufacturing technology: the status, applications, and prospects. Int J Adv Manuf Technol 97:147–161. https://doi.org/10.1007/s00170-018-1932-y
7. Guo N, Leu MC (2013) Additive manufacturing: technology, applications and research needs. Front Mech Eng 8(3):215–243. https://doi.org/10.1007/s11465-013-0248-8
8. Yuan S, Shen F, Chua CK et al (2019) Polymeric composites for powder-based additive manufacturing: materials and applications. Prog Polym Sci 91:141–168. https://doi.org/10.1016/j.progpolymsci.2018.11.001
9. Ahangar P, Cooke ME, Weber MH et al (2019) Current biomedical applications of 3D printing and additive manufacturing. Appl Sci 9(8):1713. https://doi.org/10.3390/app9081713
10. Durakovic B (2018) Design for additive manufacturing: benefits, trends and challenges. Period Eng Nat Sci 6(2):179–191. https://doi.org/10.21533/pen.v6i2.224
11. Jiménez M, Romero L, Domínguez IA et al (2019) Additive manufacturing technologies: an overview about 3D printing methods and future prospects. Complexity 2019:9656938. https://doi.org/10.1155/2019/9656938
12. Praveena BA, Lokesh N, Buradi A et al (2022) A comprehensive review of emerging additive manufacturing (3D printing technology): methods, materials, applications, challenges, trends and future potential. Mater Today Proc 52:1309–1313. https://doi.org/10.1016/j.matpr.2021.11.059
13. Beyer C (2014) Strategic implications of current trends in additive manufacturing. J Manuf Sci Eng 136:064701. https://doi.org/10.1115/1.4028599
14. Ferro C, Grassi R, Seclì C et al (2016) Additive manufacturing offers new opportunities in UAV research. Procedia CIRP 41:1004–1010. https://doi.org/10.1016/j.procir.2015.12.104
15. Solomon IJ, Sevvel P, Gunasekaran J (2021) A review on the various processing parameters in FDM. Mater Today Proc 37:509–514. https://doi.org/10.1016/j.matpr.2020.05.484
16. Nuñez PJ, Rivas A, García-Plaza E et al (2015) Dimensional and surface texture characterization in fused deposition modelling (FDM) with ABS plus. Procedia Eng 132:856–863. https://doi.org/10.1016/j.proeng.2015.12.570
17. Weng Z, Wang J, Senthil T et al (2016) Mechanical and thermal properties of ABS/montmorillonite nanocomposites for fused deposition modeling 3D printing. Mater Des 102:276–283. https://doi.org/10.1016/j.matdes.2016.04.045
18. Cuiffo MA, Snyder J, Elliott AM et al (2017) Impact of the fused deposition (FDM) printing process on polylactic acid (PLA) chemistry and structure. Appl Sci 7(6):579. https://doi.org/10.3390/app7060579
19. Knoop F, Schoeppner V (2015) Mechanical and thermal properties of FDM parts manufactured with polyamide 12. 2015 International solid freeform fabrication symposium. 935–948. https://hdl.handle.net/2152/89391
20. Xiao J, Gao Y (2017) The manufacture of 3D printing of medical grade TPU. Prog Addit Manuf 2:117–123. https://doi.org/10.1007/s40964-017-0023-1
21. Struz J, Trochta M, Hruzik L et al (2024) Wear and dynamic mechanical analysis (DMA) of samples produced via fused deposition modelling (FDM) 3D printing method. Polymers 16(21):3018. https://doi.org/10.3390/polym16213018
22. Ruiz-González S, Navarro-Lorbés P, Pascual-Martínez A et al (2024) Eco-design applied to FDM 3D printing technology. In: The 5th international conference in electronic engineering, information technology & education (EEITE), Chania, Greece, pp. 1–6. https://doi.org/10.1109/EEITE61750.2024.10654395
23. Valerga AP, Batista M, Salguero J et al (2018) Influence of PLA filament conditions on characteristics of FDM parts. Materials 11(8):1322. https://doi.org/10.3390/ma11081322
24. Flórez M, Cazón P, Vázquez M (2023) Selected biopolymers' processing and their applications: a review. Polymers 15(3):641. https://doi.org/10.3390/polym15030641
25. Van De Velde K, Kiekens P (2002) Biopolymers: overview of several properties and consequences on their applications. Polym Test 21:433–442. https://doi.org/10.1016/s0142-9418(01)00107-6
26. Schnepp Z (2013) Biopolymers as a flexible resource for nanochemistry. Angew Chem Int Ed 52:1096–1108. https://doi.org/10.1002/anie.201206943
27. Fijoł N, Aguilar-Sánchez A, Mathew AP (2022) 3D-printable biopolymer-based materials for water treatment: a review. Chem Eng J 430:132964. https://doi.org/10.1016/j.cej.2021.132964
28. Caputo MR, Fernández M, Aguirresarobe R et al (2023) Influence of FFF process conditions on the thermal, mechanical, and rheological properties of poly(hydroxybutyrate-co-hydroxy hexanoate). Polymers 15(8):1817. https://doi.org/10.3390/polym15081817
29. Mondragón-Herrera LI, Vargas-Coronado RF, Carrillo-Escalante H et al (2024) Mechanical, thermal, and physicochemical properties of filaments of poly(lactic acid), polyhydroxyalkanoates and their blend for additive manufacturing. Polymers 16(8):1062. https://doi.org/10.3390/polym16081062
30. Yokoyama D, Takamura A, Tsuboi Y et al (2023) Large-scale omics dataset of polymer degradation provides robust interpretation for microbial niche and succession on different plastisphere. ISME Commun 3:54. https://doi.org/10.1038/s43705-023-00275-z
31. Mehrpouya M, Vahabi H, Barletta M et al (2021) Additive manufacturing of polyhydroxyalkanoates (PHAs) biopolymers: materials, printing techniques, and applications. Mater Sci Eng C 127:112216. https://doi.org/10.1016/j.msec.2021.112216
32. Eraslan K, Aversa C, Nofar M et al (2022) Poly(3-hydroxybutyrate-co-3-hydroxyhexanoate) (PHBH): synthesis, properties, and applications—a review. Eur Polym J 167:111044. https://doi.org/10.1016/j.eurpolymj.2022.111044
33. Kovalcik A, Sangroniz L, Kalina M et al (2020) Properties of scaffolds prepared by fused deposition modeling of poly(hydroxyalkanoates). Int J Biol Macromol 161:364–376. https://doi.org/10.1016/j.ijbiomac.2020.06.022
34. Giubilini A, Siqueira G, Clemens FJ et al (2020) 3D-printing nanocellulose-poly(3-hydroxybutyrate-co-3-hydroxyhexanoate) biodegradable composites by fused deposition modeling. ACS Sustain Chem Eng 8:10292–10302. https://doi.org/10.1021/acssuschemeng.0c03385
35. Valentini F, Dorigato A, Rigotti D et al (2019) Polyhydroxyalkanoates/fibrillated nanocellulose composites for additive manufacturing. J Polym Environ 27:1333–1341. https://doi.org/10.1007/s10924-019-01429-8
36. Ivorra-Martinez J, Ferrer I, Aguado R et al (2023) Development of P(3HB-co-3HHx) nanohydroxyapatite (nHA) composites for scaffolds manufacturing by means of fused deposition modelling. Int J Bioprint 10:274–293. https://doi.org/10.36922/ijb.0156

37. Mori R (2023) Replacing all petroleum-based chemical products with natural biomass-based chemical products: a tutorial review. RSC Sustain 1:179–212. https://doi.org/10.1039/d2su00014h
38. Bianchi M, Dorigato A, Morreale M et al (2023) Evaluation of the physical and shape memory properties of fully biodegradable poly(lactic acid) (PLA)/poly(butylene adipate terephthalate) (PBAT) blends. Polymers 15(4):881. https://doi.org/10.3390/polym15040881
39. Weng YX, Jin YJ, Meng QY et al (2013) Biodegradation behavior of poly(butylene adipate-co-terephthalate) (PBAT), poly(lactic acid) (PLA), and their blend under soil conditions. Polym Test 32:918–926. https://doi.org/10.1016/j.polymertesting.2013.05.001
40. Sciancalepore C, Togliatti E, Giubilini A et al (2022) Preparation and characterization of innovative poly(butylene adipate terephthalate)-based biocomposites for agri-food packaging application. J Appl Polym Sci 139:52370. https://doi.org/10.1002/app.52370
41. Sciancalepore C, Togliatti E, Marozzi M et al (2022) Flexible PBAT-based composite filaments for tunable FDM 3D printing. ACS Appl Bio Mater 5:3219–3229. https://doi.org/10.1021/acsabm.2c00203
42. Yu W, Li M, Lei W et al (2024) FDM 3D printing and properties of PBAT/PLA blends. Polymers 16(8):1140. https://doi.org/10.3390/polym16081140
43. Zhang Z, He F, Wang B et al (2021) Biodegradable PGA/PBAT blends for 3D printing: material performance and periodic minimal surface structures. Polymers 13(21):3757. https://doi.org/10.3390/polym13213757
44. Jeffri NI, Nurul Fazita MR, Leh CP et al (2023) Processing and characterization of poly(hydroxybutyrate) (PHB) and poly(butylene-co-adipate-terephthalate) (PBAT) blends for fused deposition modeling (FDM) 3D printing. In: Chow WS, Jaafar M, Ariff ZM et al (eds) Proceedings of the 19th Asian workshop on polymer processing (AWPP 2022). Springer Proceedings in Materials, vol 24. Springer, Singapore. https://doi.org/10.1007/978-981-99-2015-0_2
45. Ali S, Deiab I, Pervaiz S (2025) Optimizing the properties of PHBV/PBAT blend for additive manufacturing. Procedia CIRP 131:7–12. https://doi.org/10.1016/j.procir.2024.09.004
46. Apicella A, Scarfato P, Incarnato L (2025) Study on 3D printability of PLA/PBAT/PHBV biodegradable blends for packaging applications. Polym Test 145:108748. https://doi.org/10.1016/j.polymertesting.2025.108748
47. Laycock B, Arcos-Hernandez MV, Langford A et al (2014) Crystallisation and fractionation of selected polyhydroxyalkanoates produced from mixed cultures. N Biotechnol 31:345–356. https://doi.org/10.1016/j.nbt.2013.05.005
48. Anderson KS, Schreck KM, Hillmyer MA (2008) Toughening polylactide. Polym Rev 48:85–108. https://doi.org/10.1080/15583720701834216
49. Huang F, Wu L, Li BG (2020) Sulfonated biodegradable PBAT copolyesters with improved gas barrier properties and excellent water dispersibility: from synthesis to structure-property. Polym Degrad Stab 182:109391. https://doi.org/10.1016/j.polymdegradstab.2020.109391
50. Giubilini A, Colucci G, De Trane G et al (2023) Novel 3D printable bio-based and biodegradable poly(3-hydroxybutyrate-co-3-hydroxyhexanoate) microspheres for selective laser sintering applications. Mater Today Sustain 22:100379. https://doi.org/10.1016/j.mtsust.2023.100379
51. Colucci G, Piano M, Lupone F et al (2023) Preparation and 3D printability study of bio-based PBAT powder for selective laser sintering additive manufacturing. Mater Today Chem 33:101687. https://doi.org/10.1016/j.mtchem.2023.101687
52. Gace MT, Quinn EC, Shariatikia F et al (2025) Synergistic engineering of poly(3-hydroxybutyrate) architecture and stereomicrostructure achieves enhanced material properties. Polym Chem 16:4557. https://doi.org/10.1039/d5py00691k
53. Zubkiewicz A, Szymczyk A, Sablong RJ et al (2022) Bio-based aliphatic/aromatic poly(trimethylene furanoate/sebacate) random copolymers: correlation between mechanical, gas barrier performances and compostability and copolymer composition. Polym Degrad Stab 195:109800. https://doi.org/10.1016/j.polymdegradstab.2021.109800
54. Walter R, Selzer R, Gurka M et al (2020) Effect of filament quality, structure, and processing parameters on the properties of fused filament fabricated short fiber-reinforced thermoplastics. Manuf Polym Compon 2:253–302. https://doi.org/10.1016/b978-0-12-819535-2.00009-0
55. Hamat S, Ishak MR, Sapuan SM et al (2023) Influence of filament fabrication parameter on tensile strength and filament size of 3D printing PLA-3D850. Mater Today Proc 74:457–461. https://doi.org/10.1016/j.matpr.2022.11.145
56. Tsou CH, Chen ZJ, Yuan S et al (2022) The preparation and performance of poly(butylene adipate) terephthalate/corn stalk composites. Curr Res Green Sustain Chem 5:100329. https://doi.org/10.1016/j.crgsc.2022.100329
57. Selli F, Hufenus R, Gooneie A et al (2022) Structure-property relationship in melt-spun poly(hydroxybutyrate-co-3-hexanoate) monofilaments. Polymers 14(1):200. https://doi.org/10.3390/polym14010200
58. Pavon C, Aldas M, de la Rosa-Ramírez H et al (2020) Improvement of PBAT processability and mechanical performance by blending with pine resin derivatives for injection moulding rigid packaging with enhanced hydrophobicity. Polymers 12(12):2891. https://doi.org/10.3390/polym12122891
59. Rahman MS, Al-Marhubi IM, Al-Mahrouqi A (2007) Measurement of glass transition temperature by mechanical (DMTA), thermal (DSC and MDSC), water diffusion and density methods: a comparison study. Chem Phys Lett 440:372–377. https://doi.org/10.1016/j.cplett.2007.04.067
60. Gracia-Fernández CA, Gómez-Barreiro S, López-Beceiro J et al (2010) Comparative study of the dynamic glass transition temperature by DMA and TMDSC. Polym Test 29(8):1002–1006. https://doi.org/10.1016/j.polymertesting.2010.09.005

Publisher's Note Springer Nature remains neutral with regard to jurisdictional claims in published maps and institutional affiliations.



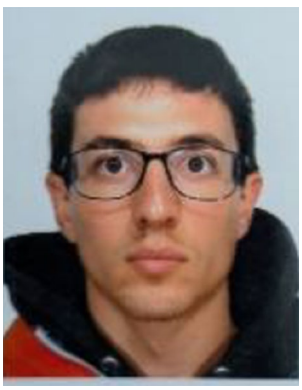
Giovanna Colucci is an assistant professor at Politecnico di Torino in Italy. Her main research topics include polymers, polymer composites obtained by additive manufacturing technologies.



Luca Fontana is a post-doctor fellow at Politecnico di Torino in Italy. His main research interest is thermoplastic polymers obtained by fused filament fabrication.



Alessandro Pegoretti is a full professor at Università di Trento in Italy. His research interests include biopolymers, polymer composites, and their mechanical properties.



Mirko Coser is a post-doctor fellow at Università di Trento in Italy. His research interests regard polymer composites, injection molding, and mechanical properties.



Massimo Messori is a full professor at Politecnico di Torino in Italy. His research topics involve biopolymers, polymer composites, and 3D printing technologies.